Indian Journal of Chemistry
Vol. 62, June 2023, pp. 586-599
DOI: 10.56042/ijc.v62i6.2522

An *in silico* design of antivirus nickel (II) complexes as therapeutic drug candidates

Sunil Kumar & Mukesh Choudhary*

Department of Chemistry, National Institute of Technology Patna, Patna 800 005, Bihar, India

E-mail: mukesh@nitp.ac.in

Received 08 July 2022; accepted(revised) 09 May 2023

A series of novel nickel (II) complexes [Ni(L^1)](**1**), [Ni(L^2)](**2**), [Ni(L^3)](**3**) and [Ni(L^4)](**4**) of salen-type Schiff base ligands (L^1H_2-L^4H_2), have been designed and synthesized, and their interaction with SARS-CoV-2 for COVID-19 and HIV virus were studied by molecular docking methods for possible therapeutic drug candidates as anti-COVID-19 and anti-HIV agents. The salen-type Schiff base ligands were condensation products of ethylene diamine with related aldehydes (3,5-Dichlorosalicylaldehyde, 5-Bromo-3-methoxy-2-hydroxy-benzaldehyde, 3,5-Diiodosalicylaldehyde, 3,5-Dinitrosalicylaldehyde). They were coordinated to metal ions through the tetradentate-N_2O_2 donor atoms. The newly synthesized complexes were fully characterized by different spectroscopic and physicochemical methods. The molecular and electronic structures of the complexes are studied by DFT based quantum chemical calculations. Additionally, inspired from recent developments to find inhibitors of the SARS-CoV-2 main protease, molecular docking studies are performed on the complexes to predict the binding mode and interactions between the ligands and the main protease of the SARS-CoV-2 (PDB ID: 7O46) for COVID-19. Also the binding potential of the nickel(II) complexes with HIV virus (PDB ID: 1UUI) are studied using in-silico molecular docking approach. The X-ray crystallographic structure of the main protease of the SARS-CoV-2 and HIV virus are retrieved from the protein data bank and used as receptor proteins. The molecular docking calculations of the nickel (II) complexes (**1**)-(**4**) with SARS-CoV-2 (PDB ID: 7O46) virus revealed the higher binding energy (-9.6 to -6.9 kcal/mol) than that of HIV virus (-9.3 to -6.7 kcal/mol) as well as docking results of chloroquine (-6.293 kcal/mol), hydroxychloroquine (-5.573 kcal/mol) and remdesivir (-6.352 kcal/mol) as anti-SARS-CoV-2 drugs. Overall, in-silico molecular docking study offers the potential role of the nickel (II) complexes as anti-COVID-19 and anti-HIV agents.

Keywords: Nickel (II) complexes, Anti-COVID-19, Anti-SARS-CoV-2, Anti-HIV, Main protease (M^{pro})

Transition metal complexes bearing salen-type ligands have been of huge importance due to their various diversified catalysis, and biological applications[1-6]. Salen metal complexes have been successfully used in alcohol oxidation and numerous organic transformation reactions because it offers both high reactivity and selectivity that includes the epoxidation of olefins, asymmetric ring-opening of epoxides which favors the formation of cyclic and linear polycarbonates[7,8]. Bis(salicylidene) ethylenediamine possess tetradentate chelating ligand that provides metal complexes of fairly rigid structure. As a result, one metal ion binds with four co-ordination sites due to availability of two nitrogen and two oxygen atoms to form three chelate rings[9,10]. Liao et. al[11] reported that intramolecular π-π stacking interactions is present between planar Schiff base ligands, which can further add to the stability of the salen-type complex. The salen type metal complexes are the building blocks of electrochemically active polymeric structures[12]. Danilova *et al.*[13] investigated the role of N_2O_2 bis-Schiff base bis-phenolate ligands as electrochemically active metallopolymers functionalized with multiple redox-active units, and showed the higher production performance into various fields such as energy storage, catalysis, electronics, or medicine. Furthermore, the salen-type complexes are conformationally flexible which shows a unique flat electron-rich aromatic surface which facilitates their interactions with nucleic acids[14,15]. Dong *et al.*[16] reported the spectroscopic behaviors of Co(II) and Cu(II) complexes with salen type bisoxime ligands. Salen type metal complexes are relevant to porphyrins but it consists of an important class of redox systems. The salen framework has exhibited high versatility for incorporation of various transition metal ions such as homogeneous catalytic asymmetric reactions[17,18]. Kochem *et al.*[19] suggested that the salen type ligand contributions to the electronic structures of the oxidized cobalt(II)salen complexes occupies

paramagnetic species containing a square pyramidal cobalt ion coordinated at the apical position by an exogenous water molecule.

Besides this, a novel coronavirus was identified as the cause of the disease which was found in the city of Wuhan, Hubei Province, China. This new virus is related to SARS-CoV (severe acute respiratory syndrome coronavirus) the causative agent of coronavirus disease 2019 (COVID-19), and declared a pandemic outbreak is the reason of the current world health crisis[20,21]. SARS-CoV-2 is a β-coronavirus belonging to the Coronaviridae family. The β-coronaviruses seriously threaten human health. Symptoms of the coronavirus disease are acute onset of fever, myalgia, dyspnea, cough, and lung opacities but currently, we do not have an effective vaccine or treatment for COVID-19 patients and continued research is urgently needed to address the challenges posed by the pandemic [22, 23].The SARS-CoV-2 main protease (M^{pro}) is not only critical for viral replication but also highly conserved in viral evolution. Therefore, M^{pro} is one of the most attractive targets for developing antiviral therapies which plays an essential role in understanding the molecular mechanism for drug discovery[24,25]. The Trans-activation Response RNA (TAR) is a viral transcript of HIV-1 which is essential for the virus to duplicate itself. Generation of acquired immunodeficiency syndrome (AIDS) in humans occurs from the destruction of macrophages and T lymphocyte cells by HIV virus type 1 (HIV-1)[26,27]. Entry of HIV virus into the host cells is a multistep process mediated essentially by viral envelope glycoprotein, which are broadly displayed at the surface of the virus. To identify new HIV reactivating agents, they are screened from microbial derived fractionating natural products library using a model of *in vitro* HIV latency as established in primary human CD4 T cells, while the HIV transcription in virus-infected cells is strongly triggered by the interaction between Tat protein and its cognate TAR RNA[28,29].

In this work, a series of new nickel (II) complexes [Ni(L^1)](**1**), [Ni(L^2)](**2**), [Ni(L^3)](**3**) and [Ni(L^4)](**4**)of salen-type Schiff base ligand (L^1H_2-L^4H_2), have been synthesised and designed as anti-COVID-19 and anti-HIV agents. The salen-type Schiff base ligands were condensation products of ethylene diamine with substituted aldehydes. They were coordinated to metal ions through the tetradentate-N_2O_2 donor atoms. The newly synthesized complexes were fully characterized by different spectroscopic and physicochemical methods. The molecular and electronic structures of the complexes are studied by DFT based quantum chemical calculations. Additionally inspired from recent developments to find inhibitors of the SARS-CoV-2 main protease, molecular docking studies are performed on the nickel(II) complexes to predict the binding mode and interactions between the ligands and the main protease of the SARS-CoV-2 (PDB ID: 7O46) for COVID-19 . Also the binding potential of the nickel(II) complexes with HIV virus (PDB ID: 1UUI) are studied using in-silico molecular docking approach. The X-ray crystallographic structure of the main protease of the SARS-CoV-2 and HIV virus are retrieved from the protein data bank and used as receptor proteins. The molecular docking calculations of the nickel (II) complexes with SARS-CoV-2 (PDB ID: 7O46) virus revealed the higher binding energy (-9.6 to -6.9 kcal/mol) than that of the HIV virus (-9.3 to -6.7 kcal/mol) as well as docking results of chloroquine (-6.293 kcal/mol), hydroxychloroquine (-5.573 kcal/mol) and remdesivir (-6.352 kcal/mol) as anti-SARS-CoV-2 drugs. Overall, in-silico molecular docking study offers the potential role of the nickel (II) complexes as anti-COVID-19 and anti-HIV agents.

Results and Discussion

Synthesis and characterization

In this work, a series of the salen-type Schiff base ligands (L^1H_2-L^4H_2) were synthesized from the condensation products of ethylene diamine with related aldehydes (3,5-Dichlorosalicylaldehyde, 5-Bromo-3-methoxy-2-hydroxy-benzaldehyde, 3,5-Diiodosalicylaldehyde, 3,5-Dinitrosalicylaldehyde). They were coordinated to metal ions through the tetradentate-N_2O_2 donor atoms. All the metal complexes were synthesized in the molar ratio of 1:1 (metal: ligand). The protocol used for their synthesis is given in Scheme 1. All the synthesized compounds were characterized with different physiochemical and spectroscopy techniques which provide evidence for their formation. Some spectral data to support the characterization of novel nickel (II) complexes [Ni(L^1)](**1**), [Ni(L^2)] (**2**), [Ni(L^3)] (**3**) and [Ni(L^4)] (**4**) are illustrated in Figures S1 to S5. The molecular structures of nickel (II) complexes are also obtained computationally (Figure S6).

The quantum computational calculations are used for structure-property relationship. Molecular docking

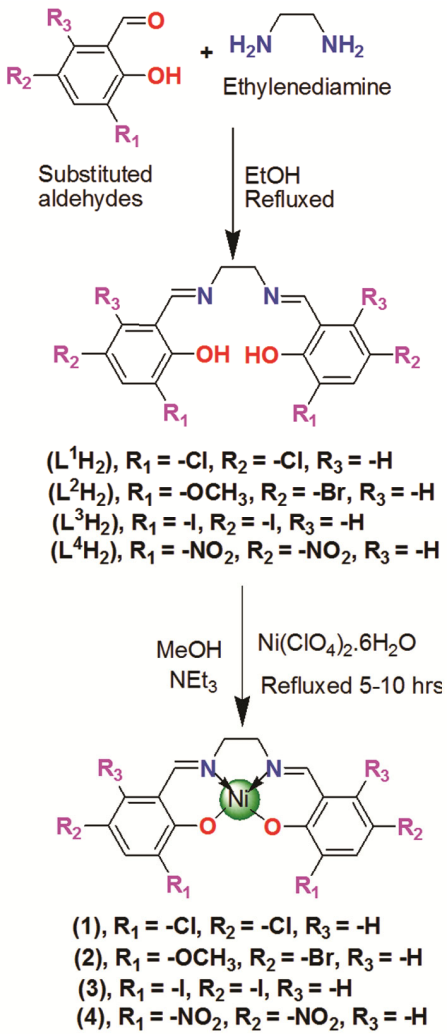

Scheme 1 — Synthetic routes for the preparation of salen-type Schiff base ligands (L^1H_2-L^4H_2) and their corresponding nickel (II) complexes [Ni(L^1)] (1), [Ni(L^2)] (2), [Ni(L^3)] (3) and [Ni(L^4)] (4).

studies are performed on the complexes to predict the binding mode and interactions between the ligands and the main protease of the SARS-CoV-2 (PDB ID: 7O46) for COVID-19. Also, the binding potential of the nickel(II) complexes (**1**)-(**4**) with HIV virus (PDB ID: 1UUI) are studied using in-silico molecular docking approach. The X-ray crystallographic structure of the main protease of the SARS-CoV-2 and HIV virus are retrieved from the protein data bank and used as receptor proteins. The molecular docking calculations of the nickel (II) complexes with SARS-CoV-2 (PDB ID: 7O46) virus revealed the higher binding energy (-9.6 to -6.9 kcal/mol) than that of HIV virus (-9.3 to -6.7 kcal/mol) as well as docking results of chloroquine (-6.293 kcal/mol), hydroxychloroquine (-5.573 kcal/mol) and remdesivir (-6.352 kcal/mol) as anti-SARS-CoV-2 drugs. This study may offer the potential role of nickel(II) complexes as new antivirus drug candidates against SARS-CoV-2 and HIV virus.

DFT based quantum computational investigation

All quantum chemical calculations were carried out using the Gaussian 09 program package[30]. DFT based quantum chemical calculations were performed on the nickel(II) complexes to get the structure property relationship. FMOs designated as LUMO and HOMO along with their orbital energies (eV) and energy gaps (eV) for the nickel(II) complexes[Ni(L^1)] (**1**), [Ni(L^2)] (**2**), [Ni(L^3)] (**3**) and [Ni(L^4)] (**4**) are shown in Figure S7 and S8. The FMOs play a very crucial role in the reactivity and stability of the complexes. Due to charge transfer and hybridization, the HOMO–LUMO gap shrinks compared to the free molecule. So the stability of the complexes (**1**)-(**4**) are proportional to the energy band gap. LUMO possess high electro-negative density but HOMO carries highly electro-positive density, while LUMO orbitals were located basically on the donor sites of the ligand/complex and HOMO orbitals are uniformly spread around the nickel (II) metal centre. Larger energy gap imparts the knowledge about the stability of the complexes. The energy gap values are summarized in Table 1. During HOMO-LUMO analysis, the relevant occupied and unoccupied Mos (HOMO/LUMO, HOMO-1/LUMO+1, HOMO-2/LUMO+2 and HOMO-3/LUMO +3) are examined. The LUMO and HOMO energies were found to be -4.625 and -1.325 eV, -6.152 eV and -1.291 eV, -6.548 and -0.892 eV, -5.324 eV and -1.913 eV for the nickel(II) complexes [Ni(L^1)] (**1**), [Ni(L^2)] (**2**), [Ni(L^3)] (**3**) and [Ni(L^4)] (**4**), rspectively. The energy gap (-3.273 eV) for [Ni(L^1)] (**1**) shows that, [Ni(L^1)] (**1**) is the most stable among all the complexes. In each nickel(II) complexes, Global reactivity descriptors (units in eV) such as ionization potential (IP), electron affinity (EA), electro negativity (χ), chemical potential (μ), global hardness (η), global softness (σ) and global electrophilicity (ω), were calculated using the formulas based on Koopmans theorem[31].

The HOMO and LUMO energies and HOMO-LUMO gap (ΔE), chemical potential (μ), global hardness (η), global softness (σ) and global electrophilicity (ω) results obtained are presented in Table 1 and Table 2. Overall electron donating and accepting abilities were described by ionization potential and electron affinity. Also, global reactivity

Table 1 — The HOMO and LUMO energies and the energy gap (ΔE)[a] of the nickel(II) complexes [Ni(L^1)] (**1**), [Ni(L^2)] (**2**), [Ni(L^3)] (**3**) and [Ni(L^4)] (**4**).

Compound	[Ni(L^1)] (**1**)	[Ni(L^2)] (**2**)	[Ni(L^3)] (**3**)	[Ni(L^4)] (**4**)
E_{LUMO}	-4.625	-6.152	-6.548	-5.324
E_{HOMO}	-1.352	-1.291	-0.892	-1.913
ÄE	-3.273	-4.862	-5.656	-3.411
$E_{LUMO\ (+1)}$	-5.968	-4.751	-4.891	-6.643
$E_{HOMO\ (-1)}$	-1.625	-2.846	-2.521	-0.785
ÄE	-4.343	-1.905	-2.370	-5.858
$E_{LUMO\ (+2)}$	-4.235	-5.146	-5.215	-4.911
$E_{HOMO\ (-2)}$	-2.315	-1.483	-1.354	-1.149
ÄE	-1.920	-3.663	-3.861	-3.762

[a] Energy gap (ΔE) = E_{LUMO}-$E_{HOMO;}$ units in eV.

Table 2 — Global reactivity descriptors of the nickel (II) salen-type complexes [Ni(L^1)](**1**), [Ni(L^2)](**2**), [Ni(L^3)](**3**) and [Ni(L^4)](**4**).

Molecular descriptors	Mathematical description	[Ni(L^1)] (1)	[Ni(L^2)] **(2)**	[Ni(L^3)] **(3)**	[Ni(L^4)] **(4)**
Ionization potential (IP)	IP = - E_{HOMO}	1.352	1.291	0.892	1.913
electron affinity (EA)	EA = -E_{LUMO}	4.625	6.152	6.548	5.324
electro negativity (÷)	÷ = (IP + EA)/2	3.002	3.721	3.720	3.618
chemical potential (ì)	ç = (IP - EA)/2	-1.636	-2.430	-2.828	-1.705
global softness (ó)	μ = -(IP + EA)/2	-3.002	-3.721	-3.720	-3.618
global hardness (ç)	ó = 1/2ç	-0.305	-0.205	-0.176	-0.293
Electrophilicity index (ù)	ù = μ^2/ 2 ç	-2.754	-33.768	-2.44	-3.838

parameter interpreted that nickel(II) complexes showed greater electron affinity (EA: 4.625, 6.152, 6.548 and 5.324 eV for complexes (**1**)-(**4**), respectively) than the ionization potential (IP: 1.352, 1.291, 0.892 and 1.913 eV for complexes (**1**)-(**4**), respectively); hence, they have greater electron accepting ability. Nevertheless, nickel(II) complexes have also expressed higher values of hardness (η =-0.176 to -0.305 eV) and a smaller value of softness (σ =-3.002 eV to -3.721 eV) suggesting that these complexes are highly stable and least reactive among all the complexes.

Furthermore, the molecular electrostatic potential maps (MEPs) is a very powerful technique which is used to predict the electrophilic and nucleophilic regions (Figure S9). The negative region (red, orange and yellow) of nickel (II) complexes occupy electrophilic sites while positive region (green, blue, pink) accompany nucleophilic sites. The MEPs exhibited the size, shape charge density and chemical reactivity of the optimized structure[32,33]. The different values of electrostatic potential are represented by different colours, with potential increases in the order: red < orange < yellow < green < blue. The red colour displays the maximum negative area, which shows favourable sites for electrophilic attack, the blue colour indicates the maximum positive area favourable for the nucleophilic attack, and the green colour represents zero potential area (Figure S9).

Furthermore, in order to have more computational insights, the net atomic charges on selected atoms of the nickel(II) complexes [Ni(L^1)] (**1**), [Ni(L^2)] (**2**), [Ni(L^3)] (**3**) and [Ni(L^4)] (**4**) were claculated through natural bonding orbital (NBO) analysis. To get insignts into the non-covalent interactions, NBO analysis will give a better understanding of the charrge transfer between the donor and acceptor moieties. Natural atomic charges on selected atoms of the nickel(II) complexes [Ni(L^1)] (**1**), [Ni(L^2)] (**2**), [Ni(L^3)] (**3**) and [Ni(L^4)] (**4**) using NBO analysis as calculated at the B3LYP/6-31G(d) level is summarized in Tables S1-S4. The summary of natural atomic charges and electron configuration (NEC) of the nickel (II) complexes (**1**)-(**4**) calculated through B3LYP/6-31G(d) level is given in Table S5. As seen in Table S5, it is concluded from the NBO results that the arrangement of core electrons, valence electrons and Rydberg electrons are consistant with calculated charges of nickel(II) central ions and also all coordination sites in ligands (H_2L^1-H_2L^4) have a calculated atomic charge and elecronic configuration lower than expected observations confirming significant electron donation from the donor atoms to the central metal atoms in the studied nickel(II) complexes. Also, the geometrical parameters of optimized ground-state geometry for the Ni(II)

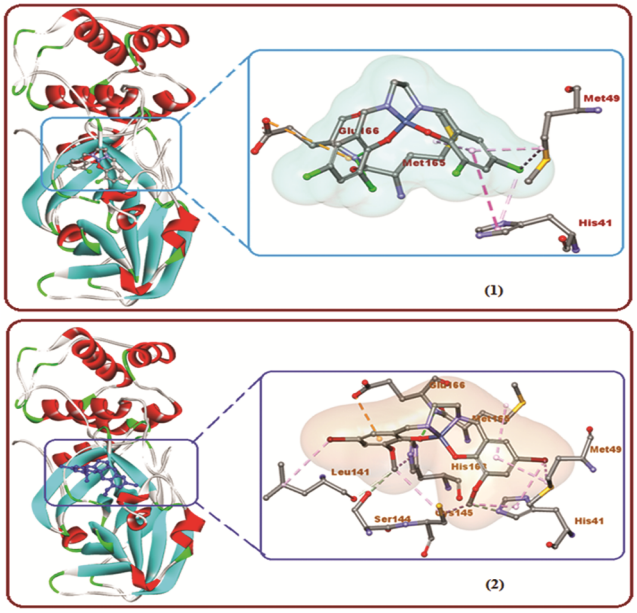

Fig. 1 — The docked nickel(II) complex [Ni(L^1)] (1) and [Ni(L^2)] (2) with SARS-CoV-2 main protease (PDB ID: 7O46) for COVID-19 with its focused view for interacting residues around the docked complexes.

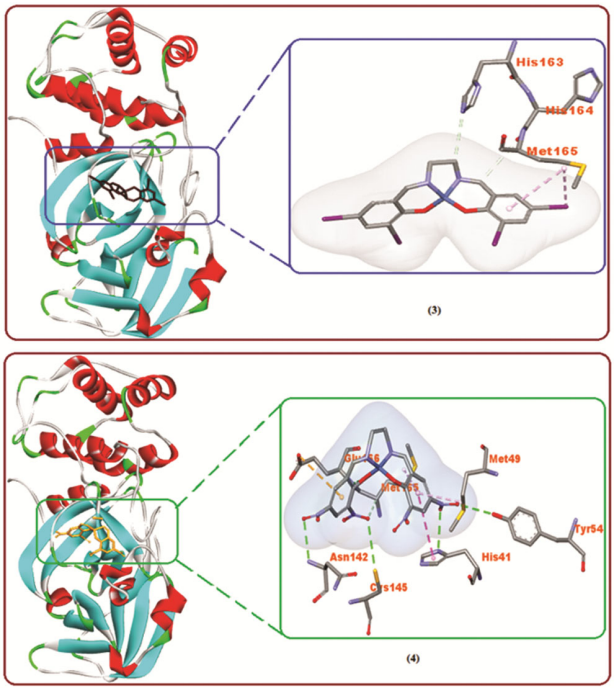

Fig. 2 — The docked nickel(II) complex [Ni(L^3)] (3) and [Ni(L^4)] (4) with SARS-CoV-2 main protease (PDB ID: 7O46) for COVID-19 with its focused view for interacting residues around the docked complexes.

complexes **(1)-(4)** calculated through the B3LYP/6-31G(d) level is tabulated in Table S6.The ground state optimized structures of the complexes is given in Figure S6.

Molecular docking with SARS-CoV-2 for COVID-19

The molecular docking is a type of bioinformatics modelling which deals with the interaction between two or more molecules to predict the protein binding geometries of compounds of a known three-dimensional structure with a target protein[34,35]. To have a deep insight about the interaction of the nickel (II) complexes [Ni(L^1)](**1**), [Ni(L^2)] (**2**), [Ni(L^3)] (**3**) and [Ni(L^4)] (**4**) with SARS-CoV-2, we have purposefully performed molecular docking analysis. Re-docking has also been performed to validate our molecular docking protocols. The aim of the study was to determine the binding energy, interacting protein residues and their corresponding distances.The in-silico molecular docking study reveals that complexes have a higher binding affinity towards COVID-19 main protease (M^{pro}) as compared to co-crystal ligands. The molecular docking studies with the crystallographic structure of SARS-CoV-2 were performed. The docked nickel(II) complexes have been performed with SARS-CoV-2 main protease (PDB ID: 7O46) with its focused view of interacting residues displayed in the Fig. 1 and Fig. 2. As the molecular docking was done to predict the binding affinity and pose of the compexes against SARS-CoV-2 main protease (PDB ID: 7O46), we have collected the molecular docking results in Table 3. The molecular docking poses of the nickel(II) complexes are displayed in Fig. 3 and Fig. 4. The effective binding affinity value of synthesized nickel(II) complexes [Ni(L^1)] (**1**), [Ni(L^2)] (**2**), [Ni(L^3)] (**3**) and [Ni(L^4)] (**4**) with SARS-CoV-2 M^{Pro} were found to be -7.4, -7.3, -6.9, -9.6 kcal/mol respectively, which makes favorable stacking interaction between receptor and complex leading to a hydrogen bond interaction, electrostatic interaction and hydrophobic contacts. When the binding energy/affinity value is more negative, the binding nature of Ni(II) salen type complexes with the SARS-CoV-2 is also greater.

In [Ni(L^1)] (**1**) complex, one hydrogen bonding interaction was found between the oxygen(O) of the phenolic moiety of salicylaldehyde region and two hydrogen atoms of the NH_2 group to the oxygen atom of GLU-166 at 3.28 Å, one electrostatic interaction was also found between oxygen of the phenolic group and the HIS-41 at 5.01 Å, which is represented by Pi-Pi T shaped dashed lines. Furthermore, two hydrophobic interactions were also found between salicylaldehyde moiety to MET-49, MET-165 at 5.22

Table 3 — The molecular docking results of the nickel (II) complexes [Ni(L^1)] (**1**), [Ni(L^2)] (**2**), [Ni(L^3)] (**3**) and [Ni(L^4)] (**4**) inside SARS-CoV-2 M^{pro} including the binding affinity, inhibition constant and different amino acid residues of M^{pro} that interact with the ligands.

Complexes		Binding affinity (kcal/mol)	Inhibition constant, Ki (μM)	Interacting protein residues		
				H-bond	Electrostatic	Hydrophobic
[Ni(L^1)] (**1**)	7O46	-7.4	1.291	GLU-166 (3.28Å)	HIS-41 (5.01Å)	MET-49 (5.22Å), MET-165 (4.99Å),
	1UUI	-7.2	6.531	A-20 (4.81Å)	C-19 (5.07Å),	G-18(3.01Å)
[Ni(L^2)] (**2**)	7O46	-7.3	3.954	GLU-166 (3.39Å) HIS-41 (4.22Å)	MET-49 (4.89Å), CYS-145 (4.46Å)	MET-165 (5.48Å), HIS-163 (4.57Å), SER-144 (3.45Å), LEU-141 (4.83Å)
	1UUI	-7.7	8.646	U-40 (2.24Å), G-26 (4.02Å)	G-28(2.91Å)	U-25(4.78Å), C-41(2.36Å), A-22(5.03Å), A-27(5.30Å)
[Ni(L^3)]	7O46	-6.9	4.225	HIS-163 (3.71Å)	MET-165 (4.82Å)	HIS-164(3.70Å)
(**3**)	1UUI	-6.7	5.537	G-21 (4.94Å)	G-18(4.83Å)	A-22(4.73Å)
[Ni(L^4)] (**4**)	7O46	-9.6	2.697	GLU-166 (3.35Å), HIS-41 (5.08Å)	MET-49 (4.72Å), TYR-54 (3.23Å)	ASN-142 (3.01Å), MET-165 (3.32Å), CYS-145 (3.67Å)
	1UUI	-9.3	1.097	A-20 (2.23Å), C-44 (2.57Å)	G-18(4.83Å)	G-17(2.35Å), C-41(3.59Å), G-43(2.23Å)

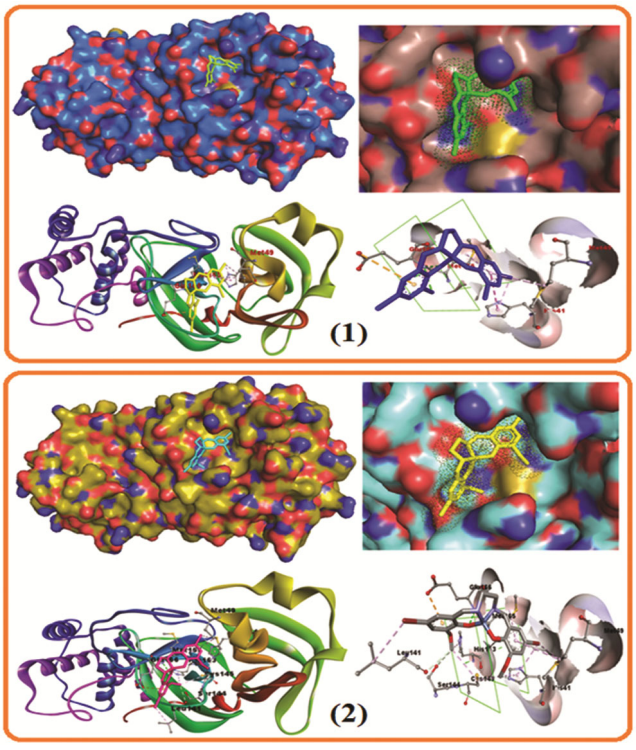

Fig. 3 — Nickel(II) complex [Ni(L^1)] (1) and [Ni(L^2)] (2) are docked into the binding cavity of the receptor protein interaction of COVID-19 M^{pro} (PDB ID: 7O46). The best docking poses of compounds in interaction with SARS-CoV-2 virus. The molecular re-docking study showed in surface view and 3D protein backbone with ligand represented as a cartoon and corresponding 2D protein-ligand interaction plot.

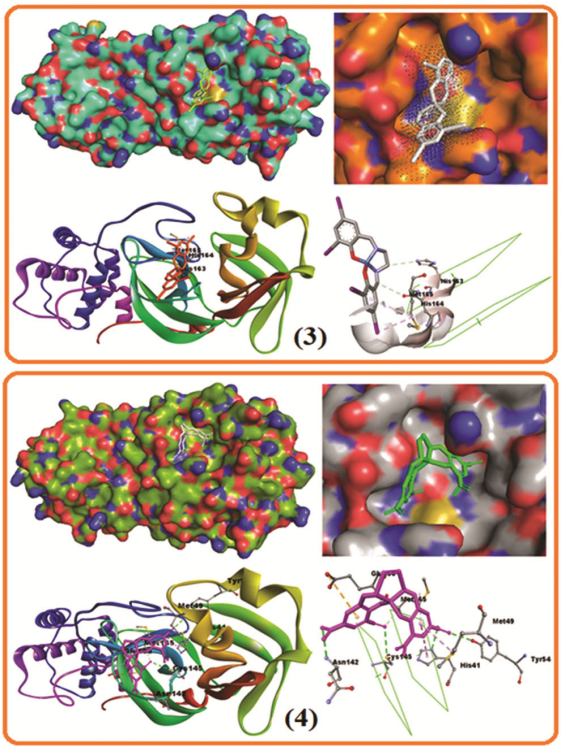

Fig. 4 — Nickel(II) complex [Ni(L^3)] (3) and [Ni(L^4)] (4) are docked into the binding cavity of the receptor protein interaction of COVID-19 M^{pro} (PDB ID: 7O46). The best docking poses of compounds in interaction with SARS-CoV-2 virus. The molecular re-docking study showed in surface view and 3D protein backbone with ligand represented as a cartoon and corresponding 2D protein-ligand interaction plot.

Å and 4.99 Å represented by alkyl as well as Pi-alkyl dashed lines. In [Ni(L^2)] (**2**) complex containing two hydrogen bonds, two electrostatic and four hydrophobic interactions, two hydrogen bonds were found between the oxygen of the phenolic salicylaldehyde moiety and carbon of OCH_3 to GLU-166 and HIS-41 at 3.39 Å and 4.22 Å, respectively which are attached through conventional/carbon hydrogen bond. Two electrostatic interactions occur between carbon of OCH_3 and bromine of salicylaldehyde moiety to CYS-145, MET-49 at 4.46 Å, 4.89 Å connected through alkyl and Pi-alkyl dashed lines, four hydrophobic interactions accommodate between carbon of OCH_3, bromine of salicylaldehyde moiety , benzene ring moiety to the SER-144, HIS-163, LEU-141, MET-165 at 3.45 Å, 4.57 Å, 4.83 Å and 5.48 Å. Similarly, [Ni(L^3)] (**3**) complex shows one hydrogen bond, one electrostatic interaction, one hydrophobic interactions where one hydrogen bond exist between the carbon of ethylene diamine region to the HIS-163 at 3.71 Å, one electrostatic interaction arise between iodine of salicylaldehyde moiety to the MET-165 at 4.82 Å through alkyl/Pi- alkyl dashed bond, one hydrophobic interaction continue with carbon of aldehyde group to the HIS-164 at 3.70 Å. Lastly two hydrogen bond interaction, two electrostatic interaction and three hydrophobic interaction were found in the case of [Ni(L^4)] (**4**) complex.

Two conventional hydrogen bonding were established between oxygen of phenolic moiety of salicylaldehyde group, oxygen of the NO_2 group to the GLU-166, HIS-41 at 3.35 Å, 5.08 Å. Two electrostatic interactions were found between the benzene ring of benzaldehyde moiety, oxygen of NO_2 group to the MET-49, TYR-54 at 4.72 Å, 3.23 Å, and three hydrophobic contacts were presented between oxygen of NO_2 group, benzene ring to ASN-142, CYS-145, MET-165 at 3.01 Å, 3.67 Å, 3.32Å. The representation of docked nickel (II) complexes [Ni(L^1)] (**1**), [Ni(L^2)] (**2**), [Ni(L^3)] (**3**) and [Ni(L^4)] (**4**) with SARS-CoV-2 M^{pro} with focussed view for interacting amino acid residues along with H-bonds and hydrophobic interactions are presented in Figures S10-S13. Besides from these, it is also very important to visualize the docking pose, 3D protein backbone, interaction plot and intermolecular interaction between the Ni(II) complexes with SARS-CoV-2 M^{Pro} for COVID-19 (PDB ID: 7O46). Fig. 5 represent the Lig-Plot which provides the automatic generation of 2D ligand/complexes protein interaction diagrams. It

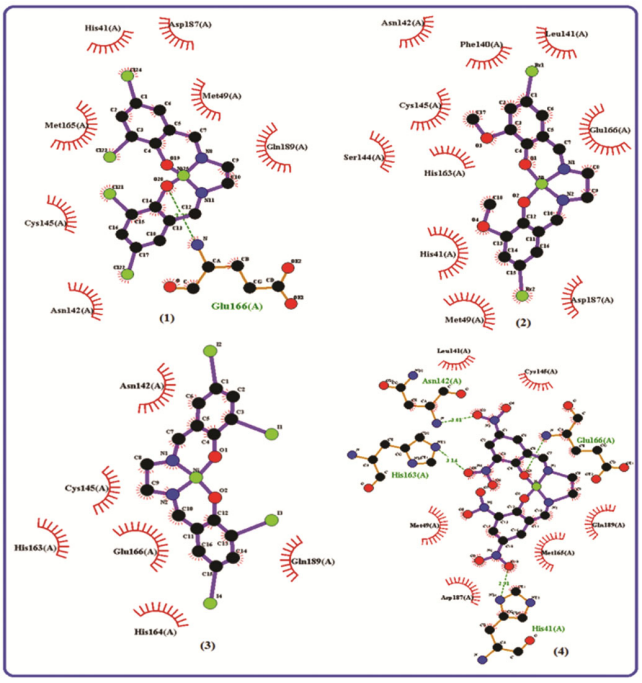

Fig. 5 — Two dimensional Lig-plot of the nickel(II) complexes [Ni(L^1)] (1), [Ni(L^2)] (2), [Ni(L^3)] (3) and [Ni(L^4)] (4) inside the SARS-CoV-2 M^{pro} (PDB ID: 7O46) for COVID-19.

is run from an intuitive java interface. The diagram shows the hydrogen bonding interaction pattern and hydrophobic contacts between the Ni(II) complexes and side chain of the receptor protein. Figure S14 shows two dimensional diagram of the nickel(II) complexes [Ni(L^1)] (**1**), [Ni(L^2)] (**2**), [Ni(L^3)] (**3**) and [Ni(L^4)] (**4**). The results obtained from molecular docking (-7.4, -7.3, -6.9, -9.6 kcal/mol for [Ni(L^1)] (**1**), [Ni(L^2)] (**2**), [Ni(L^3)] (**3**) and [Ni(L^4)] (**4**), respectively) indicates that the nickel complexes would be considered as anti-COVID-19 agents.

Ramachandran Plot study

Ramachandran plot is a central element of structural biology and is used to confirm the protein structure analysis[38] between the ligand (complex) with SARS-CoV-2 main protease (PDB ID:7O46). Ramachandran plot shows the Phi-Phi interaction torsion angles for all the residues in the crystal structure of SARS-CoV-2 main protease. Glycine residues are separately identified by triangles. The darkest area (red) corresponds to the core regions representing the most favorable combination of Phi-Psi values. Most values of ϕ and ψ are not allowed due to steric interference between non-bonded atoms. Hence, most areas of the Ramachandran plot (*i.e.*

most combinations of ϕ and ψ) represent sterically disallowed conformations of a polypeptide chain because of steric collisions between side chains and main chain. The yellow and red regions in Ramachandran plot of the complexes [Ni(L^1)] (**1**), [Ni(L^2)] (**2**), [Ni(L^3)] (**3**) and [Ni(L^4)] (**4**) with SARS-CoV-2 main protease, which signifies the generously allowed and favored regions as defined by ProCheck are presented in the Fig. 6. That regions associated with A (α helix region), B (β sheet regions), P (polyproline II region), L (left-handed helix), E (ε or extended region, lower right and upper right regions of the φ, ψ map which are accessible to glycine). The docked complexes inside the SARS-CoV-2 M^{Pro} showing the Ramachandran plot statistics is exactly 417-525 residues which covers the most favored regions containing 91-95% and the number of glycine residues units constitutes 50-60 residues which is shown as triangles but only 30-40 proline residues are involved in allowed regions shown in Fig. 6.

Main chain parameters associated with the docked complexes [Ni(L^1)] (**1**), [Ni(L^2)] (**2**), [Ni(L^3)] (**3**) and [Ni(L^4)] (**4**) inside the SARS-CoV-2 M^{pro} are displayed in Figures S15 and S16. Figures S15 and S16 show the main chain Parameter value containing percentage of residues in most favored regions showing, omega angle standard deviation, Zeta angle deviation ,hydrogen bond energy standard deviation and the overall G factor. In [Ni(L^1)] (**1**) complex one hydrogen bonding interaction was found between the

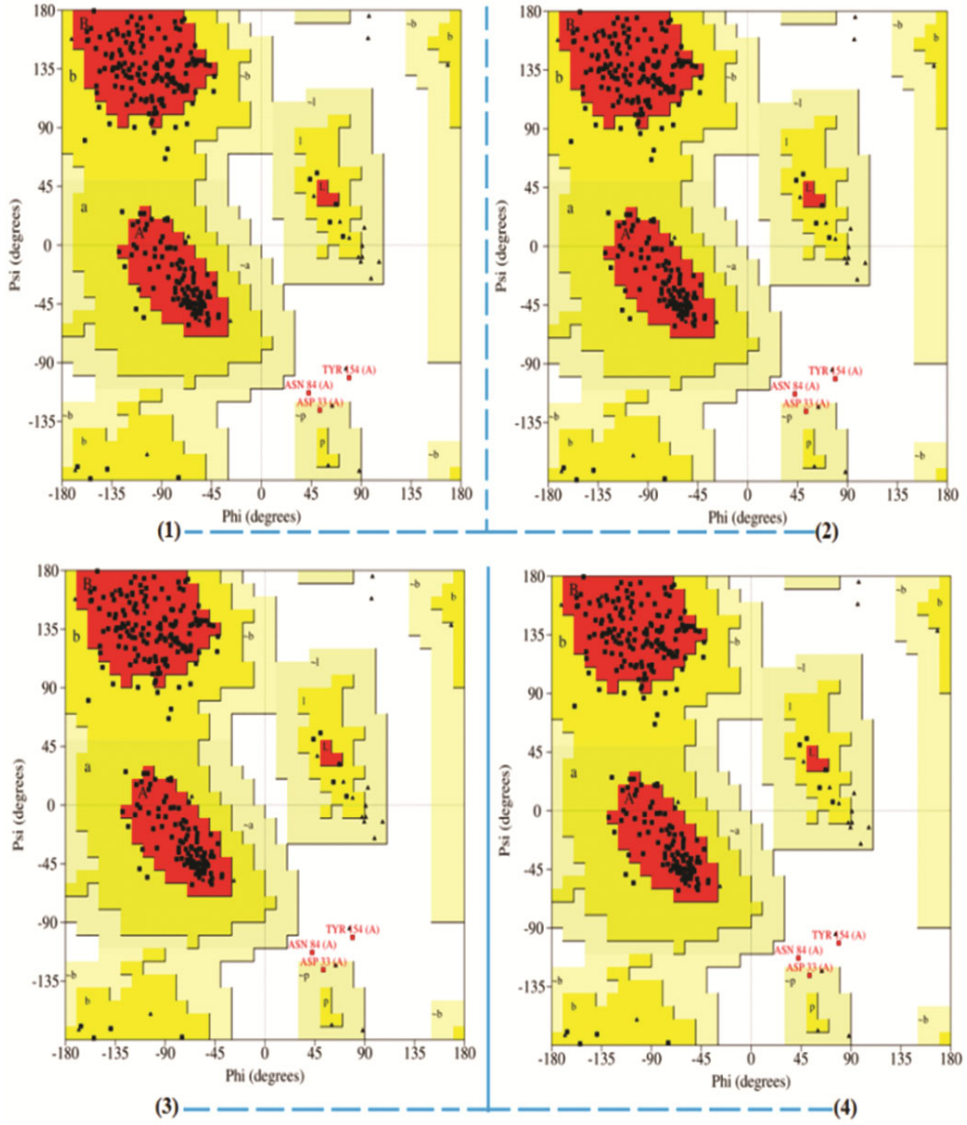

Fig. 6 — Ramachandran plot with docked nickel(II) complexes [Ni(L^1)] (1), [Ni(L^2)] (2), [Ni(L^3)] (3) and [Ni(L^4)] (4) inside the SARS-CoV-2 M^{pro} (PDB ID: 7O46) for COVID-19.

oxygen (O) of the phenolic moiety of salicylaldehyde region and two hydrogen atoms of the NH_2 group to the oxygen atom of GLU-166 at 3.28 Å, one electrostatic interaction was also found between the oxygen of the phenolic group to the HIS-41 at 5.01 Å which is represented by Pi-Pi T shaped dashed lines. Furthermore, two hydrophobic interaction were also found between salicylaldehyde moiety to MET-49, MET-165 at 5.22 Å and 4.99 Å represented by alkyl as well as Pi-alkyl dashed lines. In [Ni(L^2)] (**2**) complex containing two hydrogen bonds, two electrostatic and four hydrophobic interactions, two hydrogen bonds were found between the oxygen of the phenolic salicylaldehyde moiety and carbon of OCH_3 to GLU-166 and HIS-41 at 3.39 Å, 4.22 Å attached through conventional/ carbon hydrogen bond. Similar observations about hydrogen bond, one electrostatic interaction, one hydrophobic interactions was found for other complexes (Table 3).

Molecular docking with HIV virus

The genetic material of the virus composed of a single RNA strand which is identified as the largest among all the RNA viruses reported so far[39]. The search for new anti-HIV drugs remains a major challenge in the scientific world. To find inhibitors of HIV virus, we have purposefully performed molecular docking analysis againt HIV-1 RNA virus (PDB ID: 1UUI). Re-docking has also been performed to validate our molecular docking protocols. The aim of the study was to determine the binding energy, interacting RNA nucleotide residues and their corresponding distances. As the molecular docking was done to predict the binding affinity and pose of the complexes, the outcomes obtained from docking screening associated to the binding energy is summarized in Table 3. Fig. 7 and Fig. 8 show that the docked nickel(II) complex [Ni(L^1)] (**1**) and [Ni(L^2)] (**2**) with HIV virus (PDB ID: 1UUI) with its focused view for interacting nucleotide residues around the docked complexes. Figure S17 to S20 shows the representation of docked nickel(II) complexes [Ni(L^1)] (**1**), [Ni(L^2)] (**2**), [Ni(L^3)] (**3**) and [Ni(L^4)] (**4**) with HIV-1 RNA (PDB ID: 1UUI) with its focused view for interacting nucleotide residues along with H-bond and intermolecular interactions. The representation of docked complexes inside the HIV-1 RNA with its focused view for interacting different nucleotide residues are given in Fig. 9 and Fig. 10.

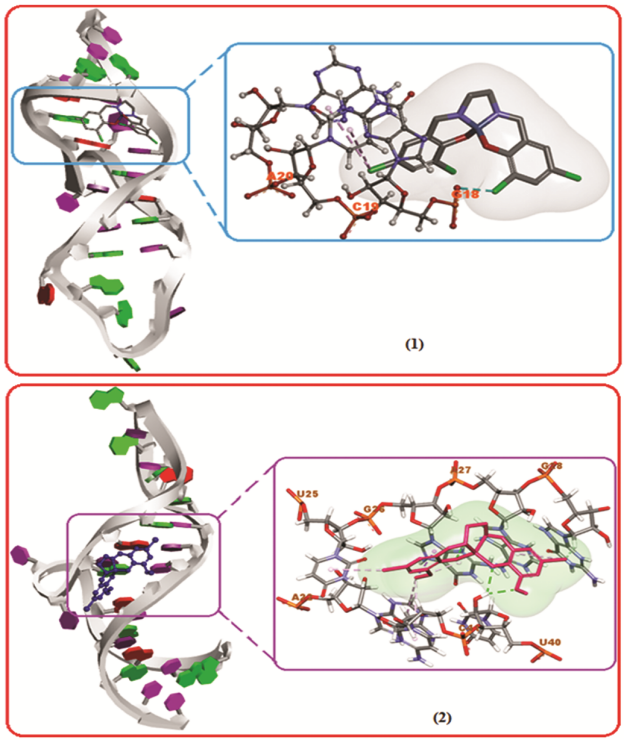

Fig. 7 — The docked nickel(II) complex [Ni(L^1)] (1) and [Ni(L^2)] (2) with HIV virus (PDB ID: 1UUI) with its focused view for interacting nucleotide residues around the docked complexes.

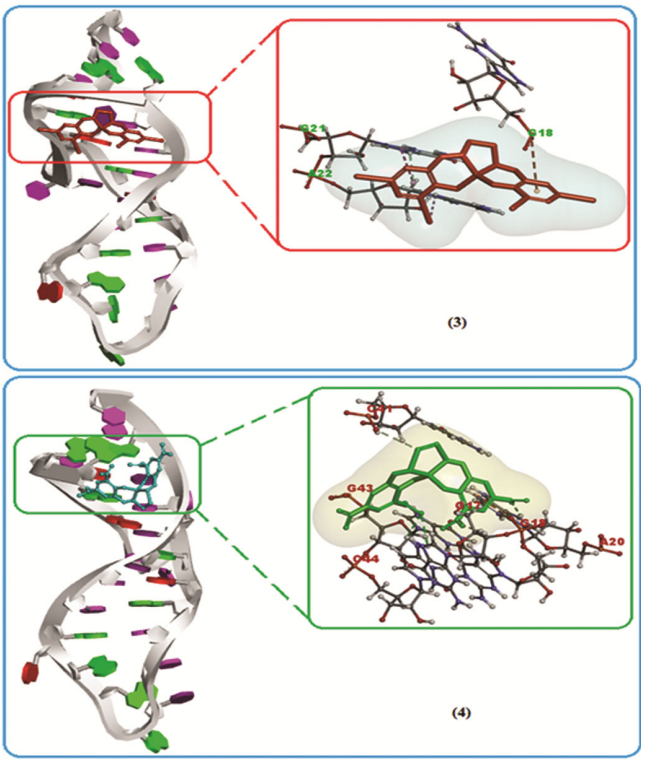

Fig. 8 — The docked nickel(II) complex [Ni(L^3)] (3) and [Ni(L^4)] (4) with HIV virus (PDB ID: 1UUI) with its focused view for interacting nucleotide residues around the docked complexes.

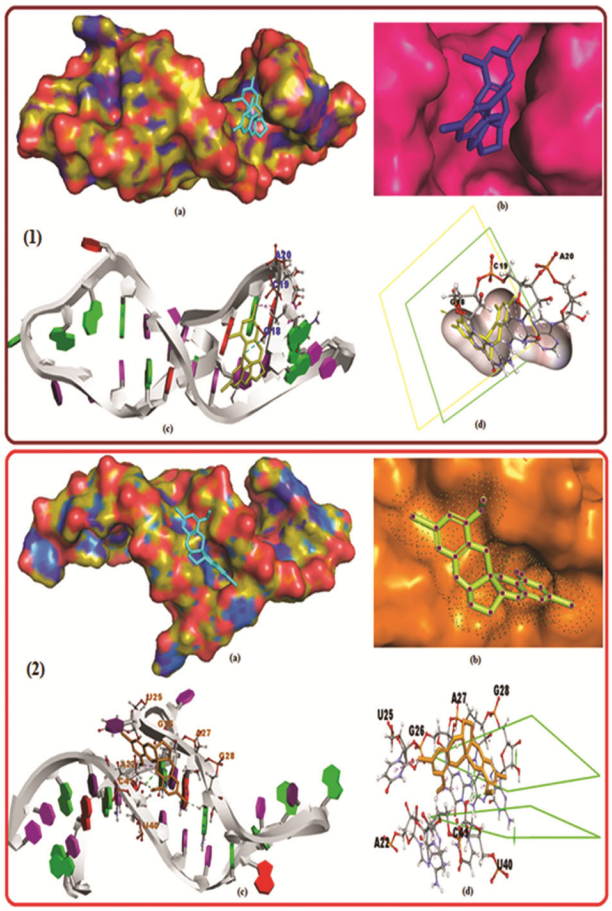

Fig. 9 — Nickel(II) complex [Ni(L^1)] (1) and [Ni(L^2)] (2) are docked into the binding cavity of the receptor protein interaction of HIV virus (PDB ID: 1UUI). The best docking poses of compounds in nucleotide interaction with HIV virus. The molecular re-docking study showed in surface view and 3D protein backbone with ligand represented as a cartoon and corresponding 2D protein-ligand interaction plot.

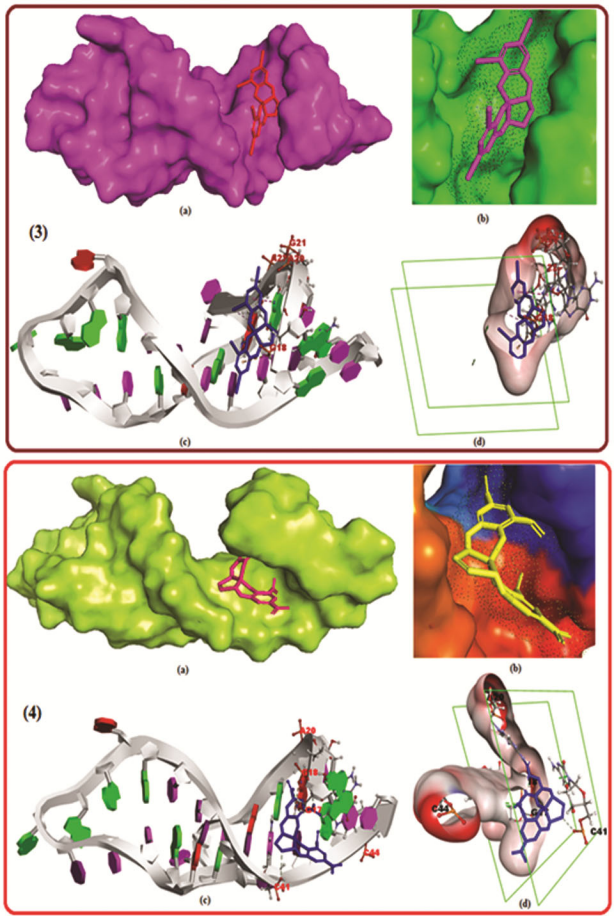

Fig. 10 — Nickel(II) complex [Ni(L^3)] (3) and [Ni(L^4)] (4) are docked into the binding cavity of the receptor protein interaction of HIV virus (PDB ID: 1UUI). The best docking poses of compounds in nucleotide interaction with HIV virus. The molecular re-docking study showed in surface view and 3D protein backbone with ligand represented as a cartoon and corresponding 2D protein-ligand interaction plot.

Fig. 11 shows the molecular re-docking of the complexes with focused view for nucleotide (RNA) interacting residues as Adenine (A), Guanine (G), Cytosine (C) and Uracil (U) of HIV-1 virus (PDB ID: 1UUI) around the docked ligands. The best docking poses of the complexes [Ni(L^1)] (**1**), [Ni(L^2)] (**2**), [Ni(L^3)] (**3**) and [Ni(L^4)] (**4**) in interaction with HIV-1 RNA virus showed in surface view and 3D protein backbone with compounds represented as a cartoon and corresponding protein-ligand interaction plot around the docked ligands. Selected nucleotide residue interactions between complexes and HIV-1 RNA virus (PDB ID: 1UUI) are: A-20, C-19, G-18 for [Ni(L^1)] (**1**); U-40, G-28, U-25, 4-41, A-22, A-27 for [Ni(L^2)] (**2**) ; G-21, G-18, A-22 for [Ni(L^3)] (**3**); A-20, C-44, G-18, G-17, C-41, G-43 for [Ni(L^4)] (**4**) inside the docked complexes. The stronger binding was predicted between the complexes and receptor protein through negative value of binding affinity. The molecular docking study reveals that the complex [Ni(L^1)] (**1**) exhibited the binding energy of -7.2 kcal/mol with an inhibition constant of 6.531 µM at inhibition binding site of receptor protein interaction of HIV-1 virus (PDB ID: 1UUI). In this compound, there existed one H-bond, one electrostatic interaction and one hydrophobic interactions between the HIV-1 RNA with the docked ligand complex. Similarly, the molecular docking study reveals that the other complexes [Ni(L^2)] (**2**), [Ni(L^3)] (**3**) and [Ni(L^4)] (**4**) resulted in the binding energy of -7.7, -6.7 and -9.3 kcal/mol with an inhibition constant of 8.646, 5.537 and 1.097 µM, respectively at receptor protein interaction of HIV-1 virus (PDB ID: 1UUI). This study may offer the new

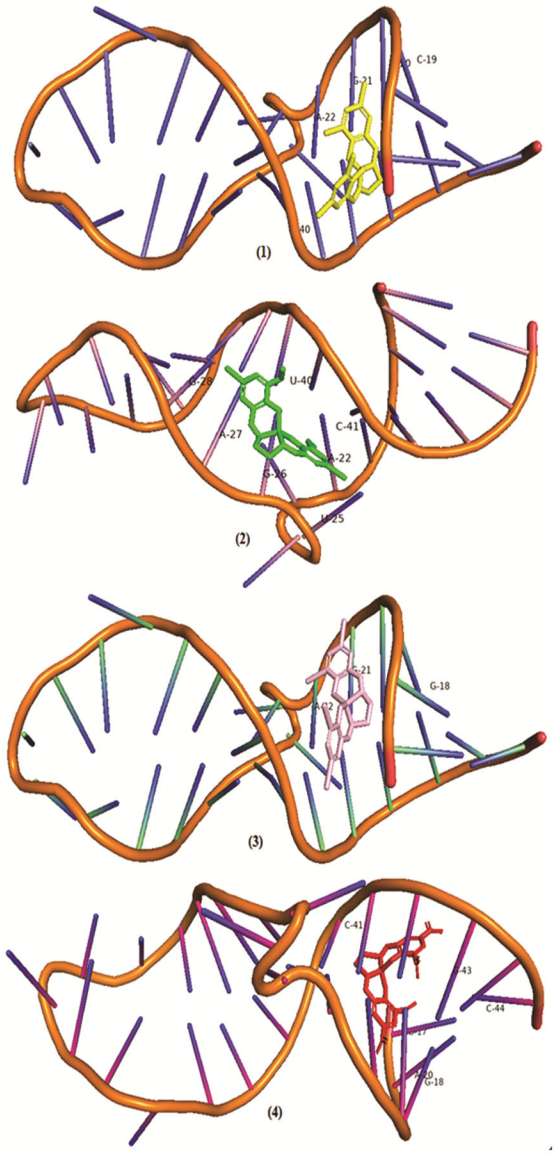

Fig. 11 — The graphical representation for the nickel(II) complexes [Ni(L^1)] (1), [Ni(L^2)] (2), [Ni(L^3)] (3) and [Ni(L^4)] (4) inside the HIV-1 RNA virus (PDB ID: 1UUI) with focused view for interacting RNA residues such as Adenine (A), Guanine (G) , Cytosine (C) and Uracil (U) around the docked complexes.

antivirus drug candidates against SARS-CoV-2 and HIV virus.

Experimental Section

Methods and Materials

The chemicals used were of AnalaR grade. Nickel(II) acetate tetrahydrate, 3,5 dichlorosalicylaldehyde, 5-Bromo-3-methoxy salicylaldehyde, 3,5 diiodosalicylaldehyde, 3,5 dinitrosalicylaldehyde, ethylenediamine were obtained from Sigma-Aldrich and were used without further purification.

Instrumentation

FT-IR and UV-Vis spectral techniques were recorded in order to confirm structural elucidation of the desired product. Elemental analytical data and quantum chemical calculations were also applied for these purposes. The FT-IR spectra of the compounds were recorded on a Shimadzu IR Affinity-1S Fourier transform infrared spectrophotometer in the range 4000-400 cm^{-1} using KBr pellets and the electronic spectra of the nickel(II) complexes were taken on a Thermo-scientific UV-Vis recording spectrophotometer Evolution-3000 in quartz cells. Melting point was measured on a Boetius micro melting point apparatus.

Quantum computational analysis

In computational chemistry, quantum mechanical methods are widely used for understanding the electronic properties, molecular orbital and molecular electrostatic properties. The electronic structure calculation of series of a new nickel (II) complexes [Ni(L^1)] (**1**), [Ni(L^2)] (**2**), [Ni(L^3)] (**3**) and [Ni(L^4)] (**4**) are carried out by the *Gaussian 09* package[30]. The PDB/Mol file formats were used for geometrical optimization for the synthesized structure. The optimization is performed using B3LYP/DFT conjugated with the mixed basis set (6-311+G(d,p)+LANL2DZ)[40]. The 6-311+G(d,p) basis set is used for non-metal atoms and LANL2DZ (Los Alamos National Laboratory 2 double) is used for the nickel metal present in the complexes. In order to get the natural charges on the atoms and its natural electronic configurations, the NBO calculations were done for the studied complexes[41,42]. All the computations were performed using the *Gaussian 09* package[30]. For each of the new nickel(II) complexes [Ni(L^1), Ni(L^2), Ni(L^3) and Ni(L^4)], HOMO-LUMO energy gap, ionization potential (IP), electron affinity (EA), electro negativity (χ), chemical potential (μ), global hardness (η), global softness (σ) and global electrophilicity (ω), were calculated from the energies of the HOMO and LUMO as reported considering Parr and Pearson's interpretation of DFT and Koopmans theorem[31]. The following equations were used to calculate Global reactivity descriptors (units in eV) by analysing molecular orbital features.

$$IP = -E_{HOMO} \quad ...(1)$$

$$EA = -E_{LUMO} \quad ...(2)$$

$$X = \frac{[IP + EA]}{2} = -\frac{[E_{LUMO} + E_{HOMO}]}{2} \quad ...(3)$$

$$\eta = \frac{[IP - EA]}{2} = -\frac{[E_{LUMO} - E_{HOMO}]}{2} \quad ...(4)$$

$$\mu = \frac{E_{HOMO} + E_{LUMO}}{2} \quad ...(5)$$

$$\sigma = \frac{1}{2\eta} \quad ...(6)$$

$$\omega = \frac{\mu^2}{2\eta} \quad ...(7)$$

Molecular docking protocols

Molecular docking studies were carried out to analyze the binding energy of a series of new nickel(II) complexes [Ni(L^1)] (**1**), [Ni(L^2)] (**2**), [Ni(L^3)] (**3**) and [Ni(L^4)] (**4**) for selected viral proteins of SARS-CoV-2 M^{pro} and HIV virus. The SARS-CoV-2 main protease was selected for molecular docking and X-ray crystallographic structure of SARS-CoV-2 M^{pro} was obtained from Protein data Bank[43] (PDB ID: 7O46; space group: C121; unit cell: a = 113.666 Å, b = 54.064 Å, c = 44.931 Å, α = 90°, β = 101.47 °, γ = 90°) and used as receptor protein. Similarly, the Human immunodeficiency virus type-1 bound to HIV-1 RNA was selected for molecular docking study. The X-ray crystallographic structure of the HIV-1 RNA virus (PDB ID: 1UUI) was also retrieved from the protein data bank and used as receptor proteins[44]. Initially, the protein coordinates were prepared by deleting all the water and heteroatoms to make the targeted protein receptor-free. Further, the polar hydrogens and Kollman charges were added to the protein using the *Autodock tool* (ADT) 1.5.6 associated[45] with *Autodock 4.2*. The prepared protein and ligand coordinates are saved in a .pdbqt file format using ADT software. The grid box of the desired volume is selected in such a way that the ligand can rotate freely inside the active site pocket protein. The configuration files are generated using the coordinates and dimension of the grid box. *Vina Lamarckian* genetic algorithm generates[46] the output files having predicted free energy for binding sites. The result comprising of different poses with corresponding energies were analyzed and high-quality figures[47] are rendered by *Biovia Discovery Studio* 2020.

General procedure for synthesis

Synthesis of Schiff base ligands (L^1H_2-L^4H_2)

A series of tetradentate-N_2O_2 Schiff base ligands (**L^1H_2-L^4H_2**) were synthesized as colored products by the refluxing 3,5-Dichlorosalicylaldehyde (20.0 mmol, 3.82 g), 5-Bromo-3-methoxysalicylaldehyde (20.0 mmol, 4.62 g), 3,5-Diiodosalicylaldehyde (20.0 mmol, 7.46 g), 3,5-Dinitrosalicylaldehyde (20.0 mmol, 4.24 g) with ethylenediamine (10.0 mmol, 0.54 ml) in 2:1 molar ratio in EtOH for 5 hrs. The coloured transparent crystalline product were obtained, which was filtered, washed with diethyl ether and stored in a desiccator over $CaCl_2$. The salen-type ligands gave satisfactory elemental analysis. L^1H_2: Colour: BrownYield: 80%. M.p.: >275 °C. Anal. Calc. for $C_{16}H_{12}Cl_4N_2O_2$ (%): C, 47.32; H, 2.98; N, 6.90. Found (%): C, 47.33; H, 2.99; N, 6.91. FAB-mass (m/z): Obs. (Calcd.) 403.97 (403.98 g/mol.). UV-Vis (MeOH) **λ** (nm): 275(π-π*) and 330 (n-π*). IR data (KBr/cm^{-1}): 1634 (>C=N); 3051 (υAr-OH), 1493 (υAr-C-C), 845 (υC-Cl). **L^2H_2**: Colour: Red,Yield: 70%. M.p.: >277 °C. Anal. Calc. for $C_{18}H_{18}Br_2N_2O_4$ (%): C, 44.47; H, 3.73; N, 5.76. Found (%): C, 44.48; H, 3.74; N, 5.75. FAB-mass (m/z): Obs. (Calcd.) 483.96 (483.98 g/mol.). UV-Vis (MeOH) **λ** (nm): 270 (π-π*) and 325 (n-π*). IR data (KBr/cm^{-1}): 1627 (>C=N); 3079 (υAr-OH), 2940 (υAr-OCH_3), 670 (υC-Br).**L^3H_2**: Colour: Orange, Yield: 72%. M.p.: >250 °C. Anal. Calc. for $C_{16}H_{12}I_4N_2O_2$ (%): C, 24.90; H, 1.57; N, 3.63. Found (%): C, 24.91; H, 1.58; N, 3.64. FAB-mass (m/z): Obs. (Calcd.) 771.71 (771.75 g/mol). UV-Vis (MeOH) **λ** (nm): 260 (π-π*) and 345 (n-π*). IR data (KBr/cm^{-1}): 1648 (>C=N); 3410 (υAr-OH), 1485(υAr-C-C), 1250, 510 (υC-I).**L^4H_2**: Colour: Dark brown Yield: 84%. M.p.: >272 °C. Anal. Calc. for $C_{16}H_{12}N_6O_{10}$ (%): C, 42.87; H, 2.70; N, 18.75. Found (%): C, 42.88; H, 2.71; N, 18.76. FAB-mass (m/z): Obs. (Calcd.) 448.06 (448.08 g/mol.). UV-Vis (MeOH) **λ** (nm): 280 (π-π*) and 335 (n-π*). IR data (KBr/cm^{-1}): 1645 (>C=N); 3415 (υAr-OH), 1525 (υAr-NO_2), 1475 (υAr-C-C).

Synthesis of nickel (II) complexes [Ni(L^1)](**1**), [Ni(L^2)](**2**), [Ni(L^3)](**3**) and [Ni(L^4)] (**4**)

A solution of $Ni(ClO_4)_2 \cdot 6H_2O$ (1.0 mmol, 0.365 g) was refluxed with MeOH solution (10 mL) of a corresponding tetradentate-N_2O_2 Schiff baseligands; L^1H_2 (1.0 mmol, 0.406 g)/ L^2H_2 (1.0 mmol, 0.486 g) / L^3H_2 (1.0 mmol, 0.771 g)/ L^4H_2 (1.0 mmol, 0.448 g) continuously for 10 -15 hrs after adding $(C_2H_5)_3N$ as base (3.0 mmol, 40 µL) was added with constant stirring the reaction mixture continuously for 5-7h at 25°C. After completion of reaction, the colored precipitates are filtered out and then dried in air at room temperature, and stored in a desiccator over

$CaCl_2$. The nickel (II) complexes gave satisfactory elemental analysis. **[Ni(L^1)]** (**1**): Colour: green,Yield: 65%. M.p.: > 280°C. Anal. Calcd. for $C_{16}H_{10}Cl_4N_2NiO_2$ (%): C, 41.53; H, 2.18; N, 6.05. Found (%): C, 41.54; H, 2.19; N, 6.06. FAB-mass (m/z): Obs. (Calcd.) 459.88 (459.0 g/mol.).UV-Vis **λ** (nm): 285 and 340 (π-π*), 430 (n-π*). IR data (KBr/cm^{-1}): 1655 (>C=N); 3352 and 1215 (υAr-OH), 775 (υC-Cl).**[Ni(L^2)]**(**2**): Colour: light green. Yield: 80%, M.p.:>290°C. Anal. Calcd. For $C_{18}H_{16}Br_2N_2NiO_4$ (**2**), (%): C, 39.83; H, 2.97; N, 5.16. Found (%): C, 39.84; H, 2.98; N, 5.17. FAB-mass (m/z): Obs. (Calcd.) 539.88 (539.40 g/mol.).UV-Vis (**λ** nm): 280 and 344 (π-π*), 440 (n-π*) IR data (KBr/cm^{-1}): 1648 (>C=N); 3443 and 1215 (deprotonated phenolic-O), 1250 (υAr-OCH_3), 770 (υC-Br), 656 (υNi-O), 517 (υNi-N). **[Ni(L^3)]** (**3**): Colour: light blue. Yield: 75%, M.p.:>285°C. Anal. Calcd. for $C_{16}H_{10}I_4N_2NiO_2$ (**3**) (%): C, 23.19; H, 1.22; N, 3.38. Found (%): C, 23.20; H, 1.23; N, 3.39. FAB-mass (m/z): Obs. (Calcd.) 827.63 (827.93 g/mol.). UV-Vis (**λ** nm): 278 and 342 (π-π*), 445 (n-π*) IR data (KBr/cm^{-1}): 1628 (>C=N); 3316 and 1218 (deprotonated phenolic-O), 1250 (υAr-OCH_3), 550 (υC-I), 652 (υNi-O), 512 (υNi-N). **[Ni(L^4)]**(**4**): Colour: light red.Yield: 65%. M.p.: > 295°C. Anal. Calcd. for $C_{16}H_{10}N_6NiO_{10}$ (**4**) (%): C, 38.06; H, 2.00; N, 16.64. Found (%): C, 38.07; H, 2.01; N, 16.65. FAB-mass (m/z): Obs. (Calcd.) 503.98 (503.00 g/mol.). UV-Vis (**λ** nm): 279 and 346 (π-π*), 448 (n-π*) IR data (KBr/cm^{-1}): 1638 (>C=N); 3410 and 1225 (deprotonated phenolic-O), 1545 (υN-O), 643 (υNi-O), 527 (υNi-N).

Conclusions

We have designed and synthesized a series of novel nickel (II) complexes [Ni(L^1)] (**1**), [Ni(L^2)] (**2**), [Ni(L^3)] (**3**) and [Ni(L^4)] (**4**) using salen-type Schiff base ligands (L^1H_2-L^4H_2). Different physiochemical and spectroscopy techniques were used to characterize the synthesized complexes which provide evidence for their formation. This work presents an in-silico design of antivirus Ni(II) complexes and their efficiency as potential candidates as therapeutic drugs. We have successfully docked all the synthesized nickel (II) complexes with the main protease (M^{Pro}) of protein of SARS-CoV-2 and HIV-1 virus. Molecular docking result reveals that all the synthesized complexes [Ni(L^1)] (**1**), [Ni(L^2)] (**2**), [Ni(L^3)] (**3**) and [Ni(L^4)] (**4**) shows higher binding energy against the main protease (M^{Pro}) of protein of SARS-CoV-2 than the HIV-1 virus. Considering all the results, it is clear that all synthesized complexes would be considered as therapeutic potential against COVID-19 and HIV virus.

Acknowledgements

The authors are thankful to the Head, Chemistry Department, National Institute of Technology Patna for providing computational resources and spectral analysis.

Supplementary Information

Supplementary information is available in the website http://nopr.niscpr.res.in/handle/123456789/58776.

Conflict of Interest

The authors declare that they have no known competing financial interests or personal relationships that could have appeared to influence the work reported in this paper.

Credit authorship contribution statement

Sunil Kumar (sunilk.phd20.ch@nitp.ac.in): Synthesis, Formal analysis and investigation, software, Writing-original draft, Resources. Mukesh Choudhary (mukesh@nitp.ac.in): Supervision, Conceptualization, Data curation, Visualization, Methodology.

References

1 Yuan Y C, Mellah M, Schulz E Z & David O R P, *Chem Rev*, 122 (2022) 8841.
2 Baleizao C & Garcia H, *Chem Rev*, 106 (2006) 3987.
3 Pratt R C, Lyons C T &Wasinger E C, *J Am Chem Soc*, 134 (2012) 7367.
4 Dong W K, Sun Y X, Zhang Y P, Li L, He X N & Tang X L, *Inorg Chim Acta*, 362 (2009) 117.
5 Pandeya S N, Sriram D, Nath G & Declercq E, *Eur J Pharmacol*, 9 (1999) 25.
6 Azam M, Dwivedi S, Resayes S I A, Adil S F, Islam M S, Kruszynska A T, Kruszynski, R & Lee D U, *J Mol Struct*,1130 (2017) 122.
7 Butsch K, Gunther T, Klein A, Stirnat K, Berkessel A & Neudorfl J, *Inorg Chim Acta*, 394 (2013) 237.
8 Brooker S, Iremonger S S & Plieger P G, *Polyhedron*, 22 (2003) 665.
9 Nasseri M A, Hemmat K & Allahresani A, *Appl Organomet Chem*, 33 (2019) e4743.
10 Mohan N, Sreejith S S, Begum P M S &Kurup M R P, *Appl Organomet Chem*, 33(2019) e5064.
11 Liao S, Yang X & Jones R A, *Cryst Growth Des*, 12 (2012) 970.
12 Shaw S & White J D, *Chem Rev*, 119 (2019) 9381.
13 Danilova J S, Avdoshenko S M, Karushev M P, Timonov A M & Dmitrieva E, *J Mol Struct*, 1241 (2021) 130668.

14 Ison E A, Cessarich J E, Du G, Fanwick P E & Omar M M A, *Inorg Chem*, 45 (2006) 2385.
15 Meermann C, Tornroos K W & Anwander R, *Inorg Chem*, 48 (2009) 2561.
16 Dong W K, Duan J G, Guan Y H, Shi J Y & Zhao C Y, *Inorg Chim Acta*, 362 (2009) 1129.
17 Kurahashi T, Hada M & Fujii H, *J Am Chem Soc*, 131 (2009) 12394.
18 Yang H Q & Chen Z X, *J Phys Chem A*, 125 (2021) 10155.
19 Kochem A, Kanso H, Baptiste B, Arora H, Philouze C, Jarjayes O, Vezin H, Luneau D, Orio M & Thomas F, *Inorg Chem*, 51 (2012) 10557.
20 Sanda M, Morrison L & Goldman R, *Anal Chem*, 93 (2021) 2003.
21 Wu F, Zhao S, Yu B, Chen Y M, Wang W, Song Z G, Hu,Y, Tao Z W, Tian J H, Pei Y Y, Yuan M L, Zhang Y L, Dai F H, Liu Y, Wang Q M, Zheng J J, Xu L, Holmes E C & Zhang Y Z, *Nature*, 579 (2020) 265.
22 Gao K, Wang R, Chen J, Tepe J J, Huang F & Wei G W, *J Med Chem*, 64 (2021) 16922.
23 Haas P, Muralidharan M, Krogan N J, Kaake R M & Huttenhain R, *J Proteome Res*, 20 (2021) 1133.
24 Chauhan D S, Prasad R, Srivastava R, Jaggi M, Chauhan S C &Yallapu M M, *Bioconjugate Chem*, 31 (2020) 2021.
25 Gahlawat A, Kumar N, Kumar R, Sandhu H, Singh I P, Singh S, Sjostedt A & Garg P, *J Chem Inf Model*, 60 (2020) 5781.
26 Leon B, Navarro G, Dickey B J, Stepan G, Tsai A, Jones G S, Morales M E, Barnes T, Ahmadyar S, Tsiang M, Geleziunas R, Cihlar T, Pagratis N, Tian Y, Yu H & Linington R G, *Org Lett*, 17 (2015) 262.
27 Kumar S, Kellish P, Robinson W E, Wang J D, Appella D H & Arya D P, *Bio Chem*, 51 (2012) 2331.
28 Sundaram R V K, Li H, Bailey L, Rashad A A, Aneja R, Weiss K, Huynh, J, Bastian A R, Papazoglou, Abrams E C, Wrenn S & Chaiken I, *BioChem*, 55 (2016) 447.
29 Krawczyk K, Sim A Y L, Knapp B, Deane C M & Minary P, *J Chem Inf Model*, 56 (2016) 1746.
30 Frisch M J, Trucks G W, Schlegel H B, Scuseria G E, Robb M A, Cheeseman J R, Scalmani G, Barone V, Mennucci B & Petersson G A, *Gaussian 16 Rev A03*, (Wallingford, CT) 2016.
31 Koopmans T, *Physica*, 1 (1934) 104.
32 Sarkar M, Nath A, Kumer A, Mallik C, Akter F, Moniruzzaman M & Ali A, *J Mol Struct*, 1244 (2021) 130953.
33 Ali M A, Nath A, Jannat M & Islam M M, *ACS omega*, 6 (2021) 25002.
34 Nath A, Kumer A, Zaben F & Khan M W, *J Basic Appl Sci*, 10 (2021) 1.
35 Nath A, Kumer A & Khan M W, *J Mol Struct*, 1224 (2021) 129225.
36 Panchariya L, Khan W A, Kuila S, Sonkar K, Sahoo S, Ghosal A, Kumar, A, Verma D K, Hasan A, Khan M A, Jain N, Mohapatra A K, Das S, Thakur J K, Maiti S, Nanda R K, Halder R, Sunil S & Arockiasamy A, *Chem Commun*, 57 (2021) 10083.
37 Ghasemi L, Esfahmi M H, Abbasi A & Behzad M, *Polyhedron*, 220 (2022) 115825.
38 Morris A, MacArthur M, Hutchinson E & Thornton J, *Proteins*, 12 (1992) 345.
39 Wang Q, Li Y, Zheng L, Huang X, Wang Y, Chen C H, Cheng Y Y, Natschke S L M & Lee K H, *ACS Med Chem Lett*, 11 (2020) 2290.
40 Kurt M, Babu P C, Sundaraganesan N, Cinar M & Karabacak M, *Spectrochim Acta Part A Mol Biomol Spectrosc*, 79 (2011) 1162.
41 Jumabaev A, Holikulov U, Hushvaktov H, Issaoui N & Absanov A, *J Mol Liq*, 377 (2023) 121552.
42 Alghamdi S K, Abbas F, Hussein R K, Alhamzani A G & El Shamy N T, *J Mol Struct*, 1271 (2023) 134001.
43 Luttens A, Gullberg H, Abdurakhmanov E, Vo D D, Akaberi D, Talibov V O, Nekhotiaeva N, Vangeel N L, Jonghe S D, Jochmans D, Krambrich J, Tas, A, Lundgren B, Gravenfors Y, Craig A J, Atilaw Y, Sandstorm A, Moodie L W K, Lundkvist A, Hemert M J V, Neyts J, Lennerstrand J, Kihlberg J, Sandberg K, Danielson U H & Carlsson J, *J Am Chem Soc*, 144 (2022) 2905.
44 Davis B, Afshar M, Varani G, Murchie A I H, Karn J, Lentzen G, Drysdale M J, Bower J, Potter A J & Aboul-Ela F, *J Mol Biol*, 336 (2004) 343.
45 Park H, Lee J & Lee S, *Proteins*, 65(2006) 549.
46 Seeliger D & Groot B L D, *J Comp Aided Mol*, 24 (2010) 417.
47 Seeliger D & Groot B L D, *J Comput Aided Mol*, 24 (2010) 417. Systèmes D, BIOVIA, Discovery Studio.